ELSEVIER

Journal of Nuclear Materials 266–269 (1999) 843–849

journal of nuclear materials

L–H transition in tokamak plasmas: 1.5-D simulations

G. Janeschitz [a,*], G.W. Pacher [b], Yu. Igitkhanov [a], H.D. Pacher [c], S.D. Pinches [d], O. Pogutse [e], M. Sugihara [a]

[a] *ITER Joint Central Team, c/o Max-Plank-Inst. Plasmaphysik, Joint Work Site, D-85748 Garching, Germany*
[b] *Centre Canadien Du Fusion Magnétique (CCFM), 1804 Montée Saint-Julie, Varennes, Que. J3X 1S1, Canada*
[c] *The NET Team, c/o Max-Planck-Institut für Plasmaphysik, Bolzmannstr. 2, D-85748 Garching, Germany*
[d] *Institut für Plasmaphysik (IPP), Bolzmannstr. 2, D-85748 Garching, Germany*
[e] *JET Joint Undertaking, Abingdon, Oxfordshire, OX 14 3EA, UK*

Abstract

Time-dependent theoretical models have been implemented in a 1.5-D transport code to describe the operational boundaries (L–H transition, ballooning limit) in terms of edge parameters. The width of the H-mode transport barrier (F. Wagner et al., Phys. Rev. Lett. 49 (1982) 1408) is self-consistently calculated and is related to α_{crit}. Access to the second stable branch of the ballooning modes is possible at high triangularity. Time dependent trajectories are calculated for several machines and the L- to H-mode transition conditions are compared with global scalings. Calibrated to one experiment (ASDEX-UP), the model yields good agreement with global scaling laws and experimental pedestal electron temperatures, and is then applied to ITER.

Keywords: H-mode; Modeling; H-mode pedestal

1. Introduction

In order to predict the behaviour of the L- to H-mode transition, the boundary conditions to be met, as well as the plasma behaviour in H-mode [1] for a reactor class machine such as ITER, a simplified physics model was developed for the H-mode pedestal region and implemented in the 1.5-D code ASTRA [2]. The starting point for this model was the work performed on the experimental plasma edge data and on the edge operational space diagram (i.e. T_e versus n_e at the plasma edge) for different confinement regimes (L-, H-mode) in the existing divertor tokamaks [3–6]. Based on this work several important observations, directing the selection of physics models for the various boundaries in the edge operational space diagram, can be made:

- The boundary for Type I ELMs is related to the ideal ballooning limit, albeit with the possibility to access the second stable branch in a small radial window in the edge pedestal area as suggested in Ref. [4] (needs shaping, i.e. $\delta_{\psi 95\%} > 0.2$).
- The boundary defining the L- to H-mode transition can be described by a critical β which in turn depends on collisionality. For a given density gradient it is thus defined by a critical temperature gradient. When knowing the H-mode pedestal width it can be expressed by a critical edge (electron) temperature measured also in L-mode at the location a-Δ_{ped} [3,6,7]. This critical temperature follows roughly a curve given by $\beta \sim C\, m_e/m_i$ at low edge densities and shows a weaker density dependence at high edge densities (hypothesis: β_{crit} increases with collisionality).
- The boundary between Type III / (Type IV) ELMs and the ELM-free or Type I ELM region seems to follow a curve which is parallel to the H-mode transition boundary albeit at higher temperature or higher β [4].
- A fourth boundary below which the onset of an X-point MARFE is observed and consequently a density limit disruption occurs can be described by a divertor detachment model [8].

Another quite striking observation is that the H-mode pedestal width seems to scale with machine size

* Corresponding author. Tel.: +49 89 3299 4111; fax: +49 89 3299 4165; e-mail: janescg@ipp-garching.mpg.de.

0022-3115/99/$ – see front matter
PII: S0022-3115(98)00615-1

[8,9]. A possible physics idea based on such a dependence, if confirmed, is that the pedestal width depends on the exact shape of the ideal ballooning limit at the plasma edge including access to the second stable branch. In this case the bootstrap and other equilibrium currents and consequently the magnetic shear profile will play a decisive role and would therefore explain the above mentioned size scaling of the pedestal width.

The above outlined interpretations of experimental observations were implemented in the ASTRA code in order to develop a time-dependent model for the L-mode, L–H transition, and H-mode behaviour and to investigate if these physics ideas are able to reproduce experimental findings. The model was tested against published edge data from various machines [8,10], as well as against global scaling laws, and was then applied to ITER parameters.

2. Physics picture of the H-mode pedestal and its implementation in ASTRA

The global physics picture of the H-mode pedestal and the L- to H-mode transition which is implemented in the 1.5-D transport code ASTRA [2] was already outlined in Ref. [10]. The main difference to this previous work is that no knowledge of the transport barrier width is assumed in the model. The main questions addressed here are the mechanism triggering the H-mode, the evolution of the transport barrier after the H-mode transition, and the width of this transport barrier.

Our hypothesis is that the L- to H-mode transition is triggered by the stabilisation of electron drift wave turbulence at the plasma edge and thus is related to a critical edge β, i.e. a critical edge (electron) temperature (at a-Δ_{ped}). This is supported by the above outlined experimental observations and by earlier work indicating that near the plasma edge the ion temperature gradient driven turbulence (ITG) becomes less important for energy transport than electron drift modes if $\lambda_T > \lambda_n$ (e.g. [11,12]) as observed in L-mode. Several theoretical models for the H-mode transition [13–19] were reviewed including those following a hypothesis different from our own. Unfortunately most of the theories do not have a simple interpretation in terms of observable plasma edge parameters [8] or do not predict the observed dependence of edge temperature versus edge density (e.g. the ones based on orbit losses). Theories pursuing the hypothesis suggested by us [14–16] are based on finite beta physics and explore the electron drift wave turbulence at the plasma edge (Alfven wave turbulence/electron modes). Two of the models [14–16] agreed reasonably well with the edge pedestal database. The model based on the electron Alfven-drift turbulence [16] was chosen for implementation into the code due to its good agreement with the experimental database and due to its relatively simple formalism.

The theory [16] suggests that the electron transport near the edge is caused by electron drift turbulence driven by inertia and dissipation. The instability can be characterised by two dimensionless parameters, the normalised beta and v_n, a normalised collisionality. At high beta, electron drift waves mix with the Alfven waves and the unstable long wavelength perturbations are suppressed when $\beta_n > \beta_{\mathrm{crit}} = 1 + v_n^{2/3}$, where

$$\beta_n = \beta\sqrt{\frac{m_i}{m_e}\frac{\lambda_{//}}{\lambda_p}} \quad v_n = v\left(\sqrt{\frac{m_i}{m_e}\frac{\lambda_{//}}{\lambda_p}}\right)^{1/2},$$

($\lambda_{//} \sim qR$, is a parallell wavelength). In our model this supplies the criterion for the L- to H-mode transition. The same theory predicts also the anomalous heat transport coefficient:

$$\chi_{\text{dr-Alfv.}} \propto \frac{D_{\text{gyro-Bohm}}}{\sqrt{\mu}} v_{\mathrm{cr}}^{1/3}\sqrt{(1+\eta^2)/\left(\frac{1}{v_{\mathrm{cr}}^2}+\eta^{4/3}\right)}, \tag{1}$$

where μ is a parallel normalised wave length ($\lambda_{n,T}(m_i/m_e))/\lambda_{//}$, $v_{\mathrm{crit}} = (1+\beta_n^2)^{-3/2}$, $\eta = v_n/v_{\mathrm{crit}}$.

Since the main emphasis was on the H-mode transport barrier, a simple transport model was applied for the plasma core ($\chi_{\text{L-mode}} = \chi_{\text{H-mode}}$ in the core), which gives L-mode confinement fitting reasonably to the H89P scaling law for the devices considered here.

$$\chi_{\mathrm{e,core}} = C_{\mathrm{core}}\frac{\sqrt{T}}{B}, \quad \chi_{\mathrm{i,core}} = 0.5C_{\mathrm{core}}\frac{\sqrt{T}}{B}. \tag{2}$$

As already stated e.g. in Ref. [19] a pressure gradient dependent radial electric field $eE = -\nabla p/n_e$. is an important factor for the transport improvements during H-mode in the pedestal region, in particular, for suppressing ion turbulence by E_r shear. Due to the moderate pressure gradients in L-mode its effect is relatively small there. However, after stabilisation of the Alfven-drift modes and the resulting increase in the edge pressure gradient it becomes an important and self-amplifying effect. The E_r shear is very important for H-mode confinement because the increasing temperature gradients and thus the increase of ITG mode turbulence (not included in the model, only χ_{core} as defined above) would otherwise cause high energy transport preventing the formation of a significant transport barrier. Combining the different contributions to the energy transport for L-mode results in

$$\chi_L = \chi_{\mathrm{neo}} + C_{\text{dr-Alfv.}}\chi_{\text{dr-Alfv}} + \chi_{\mathrm{core}}/\left(1+C_E(\nabla E)^2\right). \tag{3}$$

The boundary condition on the temperatures are $T_e = T_i = T_{2\mathrm{pt}}$, where $T_{2\mathrm{pt}}$ is calculated from a 2-point

divertor model. The constants $C_{\text{core}} = 2$ (keV$^{-0.5}$ T m^2/s), $C_{\text{dr-Alfv}} = 0.75$ and $C_{\text{E}} = 2.10^{-4}$ (m^2/keV)^2 were determined using ASDEX-Upgrade data so as to give reasonable agreement with the L–H power threshold, and with global confinement time scalings for L- and H-mode. The same constants were then used to simulate all other experiments as well as ITER.

Once the transport in the pedestal region is significantly improved, the pressure gradient starts to rise rapidly until the ideal ballooning boundary [3,4] is reached. The transport in the model is then increased such that the edge pressure gradient does not exceed this limit (simulates Type I ELMs). The related transport coefficients are:

$$\chi_{\text{ball\_e,i}} = P_{\text{e,i}}/(\nabla p_{\text{ball}} - n_{\text{e}} \nabla T_{\text{e,i}}), \tag{4}$$

where P_x is a total power across the separatrix.

The limiting pressure gradient ∇p_{ball} is calculated from an S–α model [20] using the local values of magnetic shear, aspect ratio, elongation and triangularity. In order to reproduce experimental values of pressure gradients in the edge for ASDEX-UP and JET, the α obtained from the formula is multiplied by two. The effect of a bootstrap current is included in the shear calculation, but no allowance is made for the presence of a separatrix. This approach provides a simplified implementation of ballooning mode driven Type I ELMs for plasmas with low triangularity.

However, in cases with stronger shaping (higher triangularity, e.g. in DIII-D) and at low shear values, which might result from the bootstrap current, access to second stability inside the H-mode pedestal region can occur, as suggested in Ref. [4] to explain the observed high pedestal temperatures in DIII-D. To model this effect approximately, a relation has been fitted to the results of IDBALL runs [21] which were used to map out the change in the S–α diagram versus shaping (triangularity) for a simplified equilibrium (elongated but no separatrix). The fit describes the value of the minimum shear on the S–α curve versus the triangularity δ

$$S_{\min}(\delta) \approx 0.03 + 5.08\ \delta. \tag{5}$$

The edge transport coefficients at (or beyond, for second stability) the ballooning limit are therefore

$$\chi_{\text{e,i}} = \chi_{\text{ball\_e,i}} H(S - S_{\min}) + \chi_{\text{neo\_e,i}}, \tag{6}$$

where H is the Heaviside step function and $\chi_{\text{neo-e,i}}$ the neoclassical transport coefficient. The transport is neoclassical in second stability but follows the ballooning limit in the first-stable part of the profile. Due to the interplay of triangularity, magnetic shear, the critical pressure gradient for the onset of ideal ballooning modes and the access to the second stable ballooning regime it is important to consider bootstrap currents which can develop in the pedestal region and are able to distort the magnetic shear profile considerably. The bootstrap current model included in ASTRA allows such a self-consistent modification of the magnetic shear profile, but no limit for the edge current is presently implemented in the model, such as could arise from e.g. kink modes.

Regrettably as stated in Ref. [8,9] no satisfactory model for the Type III ELMs was found so far (i.e. no model which fits the edge pedestal data for all machines) and thus they are presently not treated in the time-dependent code. The Type III ELM behaviour is important for the H- to L-mode transition because its confinement properties determine if there is a hysteresis in the H-mode power threshold or not. This is clearly seen when comparing results from ASDEX-UP [3,7] which show relatively good confinement during Type III ELMs and thus a hysteresis in the H-mode power threshold, with JET [5], which has close to L-mode confinement in the presence of Type III ELMs and therefore no hysteresis.

In addition particle transport in the rather complex plasma edge region and the question of an inward drift term and of its radial dependence is an unsolved problem. To separate the problems, a calculation of the particle transport is not carried out, but instead the density profiles are prescribed to approximate experimental observations. The density gradients used in the code for the core and for the pedestal region in L- and H-modes are listed in Table 1. The edge density gradient and the separatrix density were varied to trace out the edge operational space.

The observed steepening of the edge density gradient on transition into the H-mode was modelled by introducing a dependence on the pressure gradient, evaluated over the experimentally determined pedestal width. (This is the only place where the experimental width δ − exp enters into the simulation.) Thus

Table 1
Density profile input parameters (10^{19} m^{-3},m)

	∇n_{core}	n_{c}	∇n_{L}	∇n_{H}	n_{s}
ASDEX-UP	4.5	7	40	95	2.2
DIII-D	8.0	4	40	180	1
JET	4.5	7	40	50	2.2
ITER	0.5	11	40	50	3

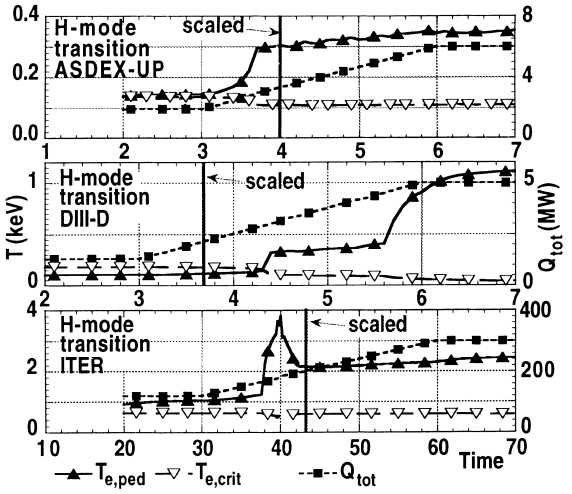

Fig. 1. Electron temperature on top of the pedestal, critical temperature for the H-mode transition, heating power, vs. time for ASDEX-UP (a), DIII-D (b) and ITER (c). Time at which the H-mode transition is expected from the scaling laws [22] is indicated by "scaled". The H-mode transition in the model (time for which the power equals the power required for the transition) is represented by the sharp increase in $T_{\mathrm{e,pedestal}}$.

$$\nabla n_{\mathrm{edge}} = \nabla n_{\mathrm{L}} + (\nabla n_{\mathrm{H}} - \nabla n_{\mathrm{L}}) \cdot \min\left[1, (\nabla p/\nabla p_{\mathrm{ball\_I}})|_{\delta-\exp}\right], \quad (7)$$

where $\nabla p_{\mathrm{ball\_I}}$ }is the ballooning limit for first stability, and

$$n_{\mathrm{edge}}(r) = n_{\mathrm{s}} + (r-a)\nabla n_{\mathrm{edge}} \quad (8)$$

The core density gradient was estimated from experimental measurements and was not varied between L- and H-mode. The transition between core and edge occurred at a defined value of density n_{c} for each machine, with a short transition region

$$n_{\mathrm{core}}(r) = n_{\mathrm{c}} + \left[r - \left(a - \frac{n_{\mathrm{s}} - n_{\mathrm{c}}}{\nabla n_{\mathrm{edge}}}\right)\right]\nabla n_{\mathrm{core}}, \quad (9)$$

$$n(r) = \left(\frac{1}{(1/n_{\mathrm{core}}(r))^{10} + (1/n_{\mathrm{edge}}(r))^{10}}\right)^{1/10}. \quad (10)$$

3. Results obtained for ASDEX-UP, DIII-D, JET and ITER

For all machines the calculations started in a 1 s (10 s for ITER) long L-mode with a heating power well below the H-mode threshold. The heating power was then ramped up over 3 s (over 30 s for ITER) to a value well above the H-mode power threshold where it was kept constant for 1 s (10 s for ITER). The density profiles evolved as described above, changing from L- to H-mode as the Alfven drift stabilised. Fig. 1(a) shows the behaviour of ASDEX-UP which is typical for all machines studied. The H-mode transition occurs where the pedestal electron temperature shows a sharp rise. In DIII-D, a second sharp rise in $T_{\mathrm{e\text{-}ped}}$ [Fig. 1(b)] occurs when second stability is obtained. ITER also transits briefly into second stability [Fig. 1(c)], but reverts soon after the H-mode transition into first stability.

The main results for all the above machines in terms of global parameters derived from the simulations are summarised in Table 2 (L-mode taken at 3 s, 30 s for ITER; H-mode taken at 7 s, 70 s for ITER, times correspond to Fig. 1). The L-mode confinement times for the existing machines follow the H-δ_{g}P scaling. However, for ITER, the L-mode confinement time predicted by the same model is quite high, H-δ_{g}P = 1.5. The power needed for the L- to H-mode transition for all machines is within ±30% of the threshold power scaling law [22]. For ITER the threshold power is −15% of the scaling law prediction (~200 MW) even at the rather high density of 1.1×10^{20} m^{-3}. In the presence of 50 : 50 D–T fuel the net additional heating power ($P_{\mathrm{threshold}} - P_{\mathrm{alpha}}$) needed to obtain an H-mode transition in ITER is thus only <50 MW. The heating power calculated does not account for radiation losses (25% in the model) which is also the case for the global scaling. In this context the result is rather optimistic because it represents only half of the total alpha heating power in an ignited ITER machine.

Due to the lack of a reliable model for Type III ELMs we can make no statement of their impact on confinement and their threshold in terms of pedestal temperature and power in ITER. The model assumes that the Type III ELM threshold can be exceeded in all machines including ITER, which results in the predicted energy confinement times during H-mode that agree

Table 2
Simulation results

	H-89P	$P_{\mathrm{LH}}/P^{\mathrm{ref}}_{\mathrm{thresh}}$.	H-97E after transition	$T_{\mathrm{e\text{-}ped}}$ (keV)	Δ_{ped} (cm)
ASDEX-UP	1.17	0.75	1.06	0.35	2–3
DIII-D	1.04	1.30	1.39	1.1	1–2
JET	1.08	0.90	1.05	1.5	3–6
ITER	1.50	0.85	0.99	2.5	10–20

again very well with the H-97E scaling (Table 2). An exception is DIII-D which shows ~35% better confinement than the global scaling, because after the H-mode transition a significant part of the pedestal enters second stability (Fig. 2). The resulting high pedestal (electron) temperature agrees well with the experimental value (Fig. 3). Without second stability, the temperature stays near half the experimental value and the width of the H-mode pedestal is wider than the experimental width. It should be noted that the transition to second stability in the code is very sensitive to input parameters, such as the prescribed edge density profile, and is only obtained by introducing a linear increase of the triangularity by 50% over the last 5% of the radius. The justification for this increase is the presence of the separatrix, and the distortion associated with it. For JET (Fig. 4) we also observe a very small region of second stability at the outboard edge of the plasma, but the global parameters are insensitive to this effect. In ITER simulations, second stability was obtained transiently during the power ramp phase [Fig. 1(c)], but the profiles re-adjust shortly after the transition and the steady-state solution is in first ballooning mode stability.

The pedestal width for the electron temperatures is determined by α_{crit} and is self-consistently calculated for all machines by the model without any further assumptions. In several test runs performed with the code it can be seen (also from Figs. 2–4) that the prescription of the density profiles do not necessarily prescribe the width of the T_e pedestal. Fig. 2 shows the comparison with ASDEX-Upgrade. The match is quite good except for some differences inside the pedestal region. It is also obvious from Fig. 3 that if the plasma is able to access the second stable branch over a significant part of the pedestal, $T_{e\text{-ped}}$ increases and the T_e-pedestal width decreases. While the calculated T_e profile is even steeper than the experimental one (Fig. 3), this behaviour reproduces quite nicely the trends which could be inferred from observations in present experiments. It explains,

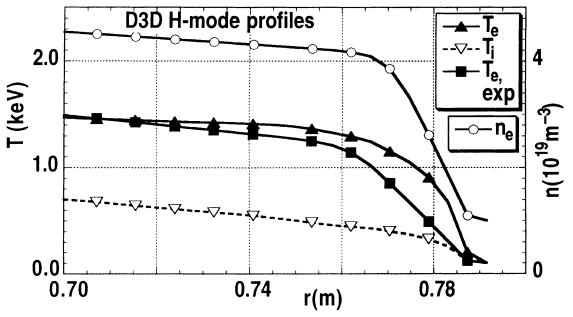

Fig. 3. Profiles of the experimental T_e (squares), the n_e used in the code (circle), the calculated T_i (open triangle) and the calculated T_e vs. minor radius for DIII-D. The steep calculated electron temperature gradient arising from the access to second stability can be seen.

for example, the differences between ASDEX-UP and DIII-D, where the pedestal width and the pedestal temperature for two similar size machines are different (Figs. 2 and 3). If however DIII-D's pedestal region is in second stability due to its stronger shaping and ASDEX-UP (low triangularity) cannot access second stability, then the differences occur naturally. A second experimental indication supporting the above physics ideas is the fact that in JET ELM free H-modes the pedestal temperatures are higher or at least comparable to ELMy H-modes, while the pedestal width is ~50% smaller [23]. This could be explained if ELM-free H-modes can access second stability, whereas the frequent ELMs in ELMy H-modes might not allow a sufficient bootstrap current to develop for shear reduction and access to second stability. This feature, however, is not implemented in the code.

Finally, the model was used to reproduce the H-mode transition and the ballooning boundary in the

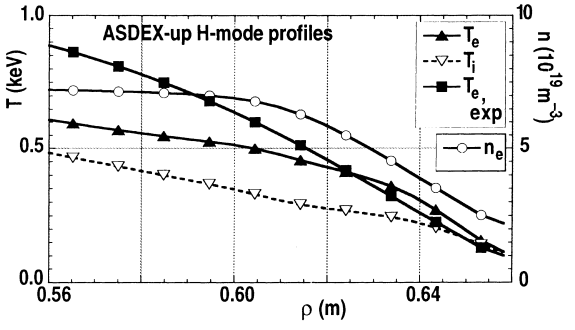

Fig. 2. Profiles of the experimental T_e (squares), the n_e used in the code (circle), the calculated T_i (open triangle) and the calculated T_e vs. minor radius for ASDEX-UP.

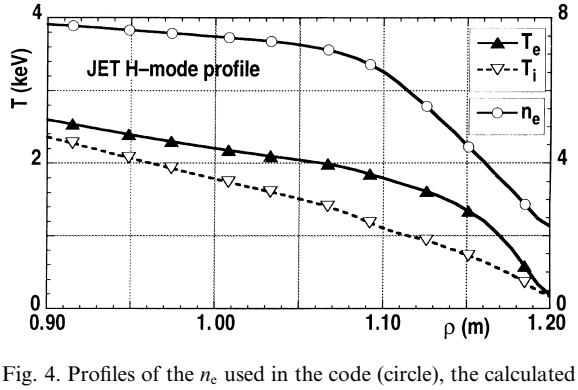

Fig. 4. Profiles of the n_e used in the code (circle), the calculated T_i (open triangle) and the calculated T_e vs. minor radius for JET. A pronounced pedestal in the electron temperature with a width comparable to the experiment can be seen [23].

edge operational space diagram and to compare the results with those obtained from the 0-D model (edge operational space diagram given by analytical formulae [8,9]). The ASDEX-UP results obtained by both methods agree rather well aside from the somewhat lower H-mode threshold derived from the 1.5-D model. In ITER the H-mode threshold calculated by the 1.5-D model is slightly higher than predicted by the 0-D model and the ballooning limit is significantly lower in the 1.5-D results. The discrepancy for the ballooning limit can be explained by the fact that in the 1.5-D model α_{crit} remains in the first stable regime while for the 0-D model an enhancement of α with triangularity was assumed [8], i.e. access to second stability over part of the pedestal. However, the 1.5-D model run for ITER also makes a brief transition into the second stable regime (Fig. 1(c)) and the resulting $T_{e\text{-}ped}$ agrees quite well with the 0-D model during this short phase. As stated above the access to second stability is rather sensitive in the model. Generally, the 0-D approach published earlier [8,9] and the 1.5-D approach for generating the edge operational space agree reasonably well, providing some confidence in the predictions.

4. Discussion and conclusions

Generally, the present model does rather well in matching the trends seen in experiments as regards global confinement scalings, L–H power threshold, pedestal width, and pedestal temperature and shows that the physics ideas implemented in the ASTRA code point in the right direction for understanding H-mode behaviour. It is, however, not claimed that with such a simple model all experimental observations can be quantitatively reproduced or that the simple theoretical representations of the physics ideas do not need further improvements. The model and its results presented here should be viewed as an initial attempt to integrate the various physics effects which play a role for the formation and sustainment of H-modes and which have to be understood in order to predict the behaviour of future machines such as ITER. Therefore this work should be seen as a status report on the beginning of a probably rather lengthy development.

Major improvements are necessary, notably in the treatment of the ballooning boundary (Eq. (4) of this paper) and second stability access. Further code runs with a stability code such as IDBALL are required, ideally including the effect of a separatrix, to determine these boundaries, so that a suitable parametrisation can be developed. The treatment of transport in second stability, as well as possible mechanisms for limiting the edge bootstrap current, i.e. the second stable region, must be evaluated and revised. A theoretical model for Type III ELMs must be developed and implemented, since this mechanism determines the hysteresis in L–H and H–L transitions. Other theoretical models for the H-mode transition trigger can be also tested if they are simple enough for implementation or if their results can be parameterised. A self-consistent model for particle transport remains to be developed, as does a better model for core energy transport.

Acknowledgements

This report is an account of work undertaken within the framework of the ITER EDA Agreement. The views and opinions expressed herein do not necessarily reflect those of the Parties to the ITER EDA Agreement, the IAEA or any agency thereof. Dissemination of the information in these papers is governed by the applicable terms of the ITER EDA Agreement.

References

[1] F. Wagner et al., Phys. Rev. Lett. 49 (1982) 1408.
[2] G.V. Pereverzev et al., ASTRA – An automatic system for transport analysis in a Tokamak, IPP Report No. 5/42, 1991.
[3] M. Kaufmann et al., 16th IAEA Fusion Energy Conference, Montreal, 1996 IAEA-F1-CN-64/O1-5.
[4] T. Osborne et al., Bulletin American Physical Society APS DPP Meeting, Denver, 1996.
[5] J. Lingertat et al., 24th EPS, Berchtesgaden, vol. 21A, Part I, 1997, p. 57.
[6] A.E. Hubbard et al., 16th IAEA Fusion Energy Conference, Montreal, 1996, IAEA-CN-64/AP2-11.
[7] W. Suttrop et al., Plasma Phys. Control. Fusion 39 (1997) 2051.
[8] G. Janeschitz et al., 24 th EPS, Berchtesgaden, vol. 21A, Part II, 1997, p. 625.
[9] Yu. Igitkhanov et al., Contrib. Plasma Phys. 38 (1997) 73.
[10] Yu. Igitkhanov et al., IAEA TCM on H-modes, Kloster Seeon, Germany, 1997.
[11] H. Nordmann, J. Weiland, Nucl. Fusion 29 (2) (1989) 251–263.
[12] R.D. Durst, R.J. Fonck, J.S. Kim, S.F. Paul, N. Bretz, C. Bush, Z. Chang, R. Hulse, Phys. Rev. Lett. 71 (1993) 3135.
[13] P.H. Diamond et al., Phys. Rev. Lett. 72 (1994) 2565.
[14] B. Rogers, J. Drake, Phys. Rev. Lett. 79 (1997) 229.
[15] B. Scott et al., 16th IAEA Fusion Energy Conference, Montreal, 1996, IAEA-CN-64/DP-18.
[16] O. Pogutse, Yu. Igitkhanov et al., 24th EPS, Berchtesgaden, vol. 21A, Part III, 1997, p. 1041.
[17] S.I. Itoh et al., Phys. Rev. Lett. 67 (1991) 2485.
[18] D. Biskamp et al., Phys. Rev. Lett. 43 (1995) 706.
[19] K. Burrel et al., Plasma Phys. Control. Fusion 34 (1992) 1859.
[20] O. Pogutse et al., Ballooning effects and plasma stability in Tokamaks, in: M. Leontovich (Ed.), Reviews of Plasma Physics, Consultants Bureau, New York, vol. 11, 1986, pp. 65-9148.

[21] The IDBALL Ideal Ballooning code, developed by UK-AEA Fusion, Culham Science Centre, Oxon, UK.
[22] J.A. Snipes et al., 24th EPS, Berchtesgaden, vol. 21A, Part III, 1997, p. 961.
[23] P. Breger et al., 24th EPS, Berchtesgaden, vol. 21A, Part I, 1997, p. 69.